Multiobjective Optimum Design of a 3-R̲RR Spherical Parallel Manipulator with Kinematic and Dynamic Dexterities

Guanglei Wu [1]

[1] *Department of Mechanical and Manufacturing Engineering, Aalborg University, 9220 Aalborg, Denmark.*
E-mail: gwu@m-tech.aau.dk

Abstract

This paper deals with the kinematic synthesis problem of a 3-R̲RR spherical parallel manipulator, based on the evaluation criteria of the kinematic, kinetostatic and dynamic performances of the manipulator. A multiobjective optimization problem is formulated to optimize the structural and geometric parameters of the spherical parallel manipulator. The proposed approach is illustrated with the optimum design of a special spherical parallel manipulator with unlimited rolling motion. The corresponding optimization problem aims to maximize the kinematic and dynamic dexterities over its regular shaped workspace.

Keywords: Spherical parallel manipulator, multiobjective optimization, Cartesian stiffness matrix, dexterity, Generalized Inertia Ellipsoid

1 Introduction

A three Degrees of Freedom (3-DOF) spherical parallel manipulator (SPM) is generally composed of two pyramid-shaped platforms, namely, a mobile platform (MP) and a fixed base that are connected together by three identical legs, each one consisting of two curved links and three revolute joints. The axes of all joints intersect at a common point, namely, the center of rotation. Such a spherical parallel manipulator provides a three degrees of freedom rotational motion. Most of the SPMs find their applications as orienting devices, such as camera orienting and medical instrument alignment (Gosselin and Hamel, 1994; Li and Payandeh, 2002; Cavallo and Michelini, 2004; Chaker et al., 2012). Besides, they can also be used to develop active spherical manipulators, i.e., wrist joint (Asada and Granito, 1985).

In designing parallel manipulators, a fundamental problem is that their performance heavily depends on their geometry (Hay and Snyman, 2004) and the mu-tual dependency of the performance measures. The manipulator performance depends on its dimensions while the mutual dependency among the performances is related to manipulator applications (Merlet, 2006b). The evaluation criteria for design optimization can be classified into two groups: one relates to the kinematic performance of the manipulator while the other relates to the kinetostatic/dynamic performance of the manipulator (Caro et al., 2011). In the kinematic considerations, a common concern is the workspace (Merlet, 2006a; Kong and Gosselin, 2004; Liu et al., 2000; Bonev and Gosselin, 2006). The size and shape of the workspace are of primary importance. Workspace based design optimization can usually be solved with two different formulations, the first formulation aiming to design a manipulator whose workspace contains a prescribed workspace (Hay and Snyman, 2004) and the second approach being to design a manipulator whose workspace is as large as possible (Lou et al., 2005). In Ref. (Bai, 2010), the SPM dexterity was optimized within a prescribed workspace by identifying
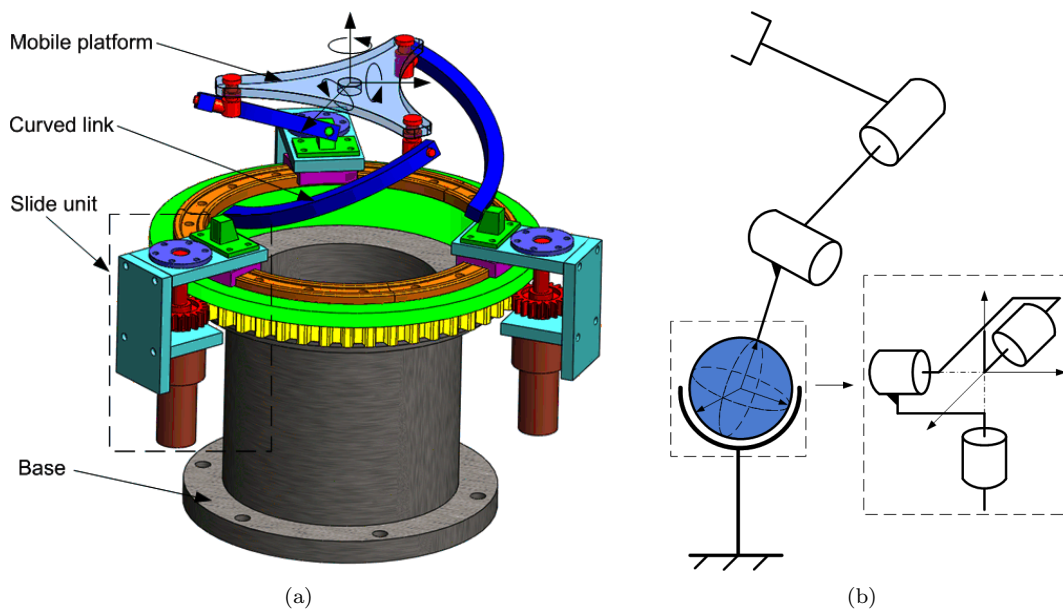
Figure 1: 3-R̲RR unlimited-roll SPM: (a) CAD model, (b) application as spherically actuated joint.

the design space. It is known from (Gosselin and Angeles, 1989) that the orientation workspace of a SPM is a maximum when the geometric angles of the links are equal to 90°. However, maximizing the workspace may lead to a poor design with regard to the manipulator dexterity and manipulability (Stamper et al., 1997; Durand and Reboulet, 1997). This problem can be solved by properly defining the constraints on dexterity (Merlet, 2006a; Huang et al., 2003). For the optimum design of SPMs, a number of works focusing on the kinematic performance, mainly the dexterity and workspace, have been reported, whereas, the kinetostatic/dynamic aspects receive relatively less attention. In general, the design process simultaneously deals with the two previously mentioned groups, both of which include a number of performance measures that essentially vary throughout the workspace. On the kinetostatic aspect, the SPM stiffness is an important consideration (Liu et al., 2000) to characterize its elastostatic performance. When they are used to develop spherically actuated joint, not only the MP angular displacement but also the translational displacement of the rotation center should be evaluated from the Cartesian stiffness matrix of the manipulator and should be minimized. Moreover, the dynamic performance of the manipulator should be as high as possible.

Among the evaluation criteria for optimum geometric parameters design, an efficient approach is to solve a multiobjective optimization problem, which takes all or most of the evaluation criteria into account. As the objective functions are usually conflicting, no single solution can be achieved in this process. The solutions of such a problem are non-dominated solutions, also called Pareto-optimal solutions. Some multiobjective optimization problems of parallel manipulators (PMs) have been reported in the last few years. Hao and Merlet proposed a method different from the classical approaches to obtain all the possible design solutions that satisfy a set of compulsory design requirements, where the design space is identified via the interval analysis based approach (Hao and Merlet, 2005). Ceccarelli et al. focused on the workspace, singularity and stiffness properties to formulate a multi-criterion optimum design procedure for both parallel and serial manipulators (Ceccarelli et al., 2005). Stock and Miller formulated a weighted sum multi-criterion optimization problem with manipulability and workspace as two objective functions (Stock and Miller, 2003). Krefft and Hesselbach formulated a multi-criterion elastodynamic optimization problem for parallel mechanisms while considering workspace, velocity transmission, inertia, stiffness and the first natural frequency as optimization objectives (Krefft and Hesselbach, 2005). Altuzarra et al. dealt with the multiobjective optimum design of a parallel Schönflies motion generator, in which the manipulator workspace volume and dexterity were considered as objective functions (Altuzarra et al., 2009).

In this work, a multiobjective design optimization problem is formulated. The design optimization problem of the 3-DOF spherical parallel manipulator considers the kinematic performance, the accuracy and the dynamic dexterity of the mechanism under design. The performances of the mechanism are also optimized over a regular shaped workspace. The multiobjective de-
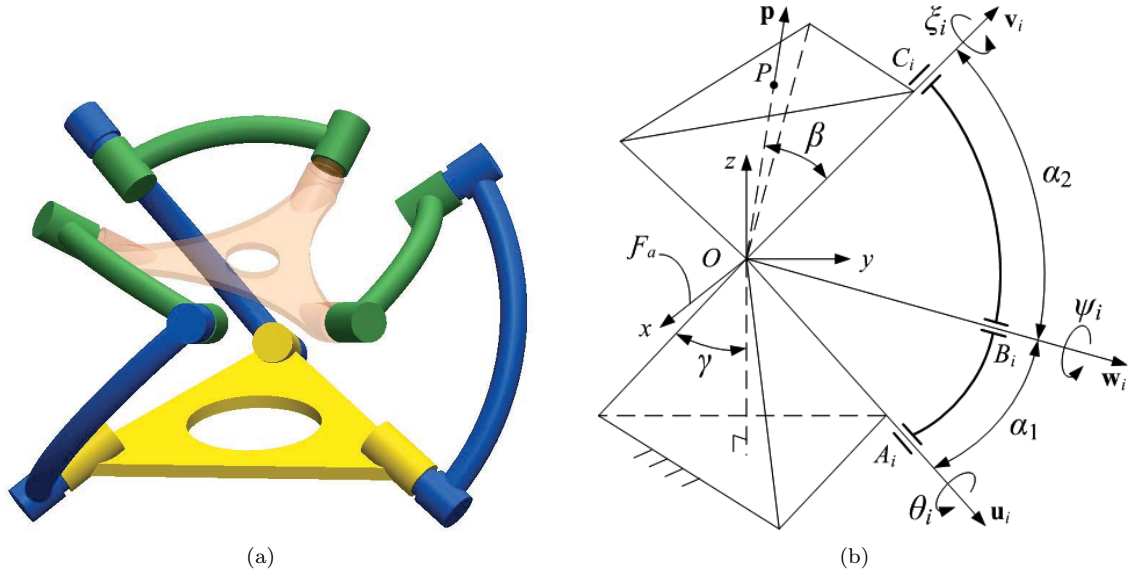
Figure 2: Architecture of a general SPM: (a) overview, (b) parameterization of the ith leg.

sign optimization problem is illustrated with a 3-$\underline{\text{R}}$RR SPM shown in Figure 1, which can replace the serial chains based wrist mechanisms. The non-dominated solutions, also called Pareto-optimal solutions, of the multiobjective optimization problem are obtained with a genetic algorithm.

2 Manipulator Architecture

The spherical parallel manipulator under study is a novel robotic wrist with an unlimited roll motion (Bai, 2010; Bai et al., 2009), which only consists of three curved links connected to a mobile platform (MP). The mobile platform is supposed to be quite stiffer than the links, which is considered as a rigid body. The three links are driven by three actuators moving independently on a circular rail of model HCR 150 from THK via pinion and gear-ring transmissions. Thanks to the circular guide, the overall stiffness of the mechanism is increased. Moreover, such a design enables the SPM to generate an unlimited rolling motion, in addition to limited pitch and yaw rotations.

A general spherical parallel manipulator is shown in Figure 2(a) (Liu et al., 2000). Figure 2(b) represents the parameters associated with the ith leg of the SPM,

$i = 1, 2, 3$. The SPM is composed of three legs that connect the mobile-platform to the base. Each leg is composed of three revolute joints. The axes of the revolute joints intersect and their unit vectors are denoted by $\mathbf{u}_i$, $\mathbf{w}_i$ and $\mathbf{v}_i$, $i = 1, 2, 3$. The arc angles of the three proximal curved links are the same and equal to α_1. Likewise, the arc angles of the three distal curved links are the same and equal to α_2. The radii of the link midcurves are the same and equal to R. Geometric angles β and γ define the geometry of the two pyramidal base and mobile platforms. The presented SPM in Figure 1(a) is a special case with $\gamma = 0$. The origin O of the reference coordinate system $\mathcal{F}_a$ is located at the center of rotation.

3 Kinematic and Kinetostatic Modeling of the SPM

The kinematics of the SPMs has been well documented (Gosselin and Angeles, 1989), which is not repeated in detail here. Hereafter, the orientation of the mobile platform is described by the orientation representation of *azimuth-tilt-torsion* $(\phi - \theta - \sigma)$ (Bonev, 2008), for which the rotation matrix is expressed as

$$\mathbf{Q} = \begin{bmatrix} \text{c}\phi\text{c}\theta\text{c}(\phi-\sigma)+\text{s}\phi\text{s}(\phi-\sigma) & \text{c}\phi\text{c}\theta\text{s}(\phi-\sigma)-\text{s}\phi\text{c}(\phi-\sigma) & \text{c}\phi\text{s}\theta \\ \text{s}\phi\text{c}\theta\text{c}(\phi-\sigma)-\text{c}\phi\text{s}(\phi-\sigma) & \text{s}\phi\text{c}\theta\text{s}(\phi-\sigma)+\text{c}\phi\text{c}(\phi-\sigma) & \text{s}\phi\text{s}\theta \\ -\text{s}\theta\text{c}(\phi-\sigma) & -\text{s}\theta\text{s}(\phi-\sigma) & \text{c}\theta \end{bmatrix} \tag{1}$$

where $\phi \in (-\pi, \pi]$, $\theta \in [0, \pi)$, $\sigma \in (-\pi, \pi]$, and $\mathrm{s}(\cdot) = \sin(\cdot)$, $\mathrm{c}(\cdot) = \cos(\cdot)$.

Under the prescribed coordinate system, unit vector $\mathbf{u}_i$ is expressed in the base frame $\mathcal{F}_a$ below:

$$\mathbf{u}_i = \begin{bmatrix} -\sin\eta_i\sin\gamma & \cos\eta_i\sin\gamma & -\cos\gamma \end{bmatrix}^T \quad (2)$$

where $\eta_i = 2(i-1)\pi/3$, $i = 1, 2, 3$.

Unit vector $\mathbf{w}_i$ of the intermediate revolute joint axis in the ith leg is expressed in $\mathcal{F}_a$ as:

$$\mathbf{w}_i = \begin{bmatrix} -\mathrm{s}\eta_i\mathrm{s}\gamma\mathrm{c}\alpha_1 + (\mathrm{c}\eta_i\mathrm{s}\theta_i - \mathrm{s}\eta_i\mathrm{c}\gamma\mathrm{c}\theta_i)\mathrm{s}\alpha_1 \\ \mathrm{c}\eta_i\mathrm{s}\gamma\mathrm{c}\alpha_1 + (\mathrm{s}\eta_i\mathrm{s}\theta_i + \mathrm{c}\eta_i\mathrm{c}\gamma\mathrm{c}\theta_i)\mathrm{s}\alpha_1 \\ -\mathrm{c}\gamma\mathrm{c}\alpha_1 + \mathrm{s}\gamma\mathrm{c}\theta_i\mathrm{s}\alpha_1 \end{bmatrix} \quad (3)$$

The unit vector $\mathbf{v}_i$ of the last revolute joint axis in the ith leg, is a function of the mobile-platform orientation, namely,

$$\mathbf{v}_i = \mathbf{Q}\mathbf{v}_i^* \quad (4)$$

where $\mathbf{v}_i^*$ corresponds to the unit vector of the last revolute joint axis in the ith leg when the mobile platform is in its home configuration:

$$\mathbf{v}_i^* = \begin{bmatrix} -\sin\eta_i\sin\beta & \cos\eta_i\sin\beta & \cos\beta \end{bmatrix}^T \quad (5)$$

3.1 Kinematic Jacobian matrix

Let $\boldsymbol{\omega}$ denote the angular velocity of the mobile-platform, the screws velocity equation via the ith leg can be stated as

$$\$_\omega = \begin{bmatrix} \boldsymbol{\omega} \\ \mathbf{0} \end{bmatrix} = \dot{\theta}_i\hat{\$}_A^i + \dot{\psi}_i\hat{\$}_B^i + \dot{\xi}_i\hat{\$}_C^i \quad (6)$$

with the screws for the revolute joints at points A_i, B_i and C_i expressed as

$$\hat{\$}_A^i = \begin{bmatrix} \mathbf{u}_i \\ \mathbf{0} \end{bmatrix}, \ \hat{\$}_B^i = \begin{bmatrix} \mathbf{w}_i \\ \mathbf{0} \end{bmatrix}, \ \hat{\$}_C^i = \begin{bmatrix} \mathbf{v}_i \\ \mathbf{0} \end{bmatrix}$$

Since the axes of the two passive revolute joints in each leg lie in the plane B_iOC_i, the following screw is reciprocal to all the revolute joint screws of the ith leg and does not lie in its constraint wrench system:

$$\hat{\$}_r^i = \begin{bmatrix} \mathbf{0} \\ \mathbf{w}_i \times \mathbf{v}_i \end{bmatrix} \quad (7)$$

Applying the orthogonal product ($\circ$) (Tsai, 1998) to both sides of Eqn. (6) yields

$$\hat{\$}_r^i \circ \$_\omega = (\mathbf{w}_i \times \mathbf{v}_i)^T \boldsymbol{\omega} = (\mathbf{u}_i \times \mathbf{w}_i) \cdot \mathbf{v}_i\dot{\theta}_i \quad (8)$$

As a consequence, the expression mapping from the mobile platform twist to the input angular velocities is stated as:

$$\mathbf{A}\boldsymbol{\omega} = \mathbf{B}\dot{\boldsymbol{\theta}} \quad (9)$$

with

$$\mathbf{A} = \begin{bmatrix} \mathbf{a}_1 & \mathbf{a}_2 & \mathbf{a}_3 \end{bmatrix}, \ \mathbf{a}_i = \mathbf{w}_i \times \mathbf{v}_i \quad (10\mathrm{a})$$

$$\mathbf{B} = \mathrm{diag}\begin{bmatrix} b_1 & b_2 & b_3 \end{bmatrix}, \ b_i = (\mathbf{u}_i \times \mathbf{w}_i) \cdot \mathbf{v}_i \quad (10\mathrm{b})$$

where $\dot{\boldsymbol{\theta}} = \begin{bmatrix} \dot{\theta}_1 & \dot{\theta}_2 & \dot{\theta}_3 \end{bmatrix}^T$. Matrices $\mathbf{A}$ and $\mathbf{B}$ are the forward and inverse Jacobian matrices of the manipulator, respectively. If $\mathbf{B}$ is nonsingular, the kinematic Jacobian matrix $\mathbf{J}$ is obtained as

$$\mathbf{J} = \mathbf{B}^{-1}\mathbf{A} \quad (11)$$

3.2 Cartesian stiffness matrix

The stiffness model of the SPM under study is established with virtual spring approach (Pashkevich et al., 2009), by considering the actuation stiffness, link deformation and the influence of the passive joints. The flexible model of the ith leg is represented in Figure 3. Figure 3(b) illustrates the link deflections and variations in passive revolute joint angles.

Let the center of rotation be the reference point of the mobile platform. Analog to Eqn. (6), the small displacement screw of the mobile-platform can be expressed as:

$$\$_O^i = \begin{bmatrix} \Delta\boldsymbol{\phi} \\ \Delta\mathbf{p} \end{bmatrix} = \Delta\theta_i\hat{\$}_A^i + \Delta\psi_i\hat{\$}_B^i + \Delta\xi_i\hat{\$}_C^i \quad (12)$$

where $\Delta\mathbf{p} = [\Delta x, \Delta y, \Delta z]^T$ is linear displacement of the rotation center and $\Delta\boldsymbol{\phi} = [\Delta\phi_x, \Delta\phi_y, \Delta\phi_z]^T$ is the MP orientation error. Note that this equation only includes the joint variations, while for the real manipulator, link deflections should be considered as well.

The screws associated with the link deflections are formulated as follows:

$$\hat{\$}_{u1}^i = \begin{bmatrix} \mathbf{r}_i \\ \mathbf{r}_C^i \times \mathbf{r}_i \end{bmatrix}, \hat{\$}_{u2}^i = \hat{\$}_C^i, \hat{\$}_{u3}^i = \begin{bmatrix} \mathbf{n}_i \\ \mathbf{r}_C^i \times \mathbf{n}_i \end{bmatrix} \quad (13)$$

$$\hat{\$}_{u4}^i = \begin{bmatrix} \mathbf{0} \\ \mathbf{r}_i \end{bmatrix}, \hat{\$}_{u5}^i = \begin{bmatrix} \mathbf{0} \\ \mathbf{v}_i \end{bmatrix}, \hat{\$}_{u6}^i = \begin{bmatrix} \mathbf{0} \\ \mathbf{n}_i \end{bmatrix}$$

where $\mathbf{n}_i = \mathbf{w}_i \times \mathbf{v}_i$ is the normal vectors of plane B_iOC_i, $\mathbf{r}_i = \mathbf{w}_i \times \mathbf{n}_i$, and $\mathbf{r}_C^i$ is the position vector of point C_i from O. The directions of the vectors $\mathbf{r}_i$ and $\mathbf{n}_i$ are identical to Δu_4^i and Δu_6^i, respectively.

By considering the link deflections $\Delta u_1^i...\Delta u_6^i$ and variations in passive joint angles and adding all the deflection freedoms to Eqn. (12), the mobile platform deflection in the ith leg is stated as

$$\begin{aligned} \$_O^i = &\Delta\theta_i\hat{\$}_A^i + \Delta\psi_i\hat{\$}_B^i + \Delta\xi_i\hat{\$}_C^i + \Delta u_1^i\hat{\$}_{u1}^i + \Delta u_2^i\hat{\$}_{u2}^i \\ &+ \Delta u_3^i\hat{\$}_{u3}^i + \Delta u_4^i\hat{\$}_{u4}^i + \Delta u_5^i\hat{\$}_{u5}^i + \Delta u_6^i\hat{\$}_{u6}^i \end{aligned} \quad (14)$$

The previous equation can be written in a compact form by separating the terms related to the variations

(a)

(b)
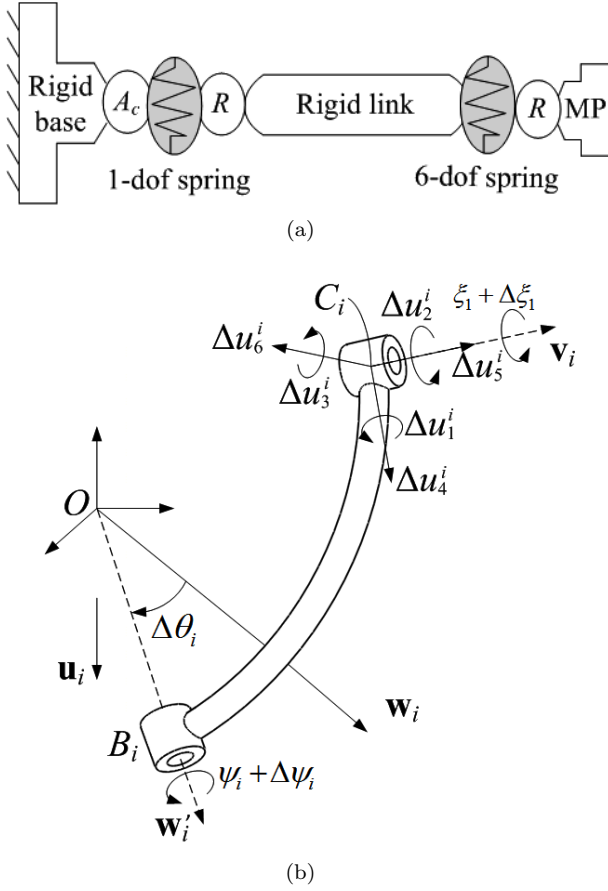
Figure 3: Flexible model of a single leg: (a) virtual spring model, where A_c stands for the actuator, R for revolute joints and MP for the mobile platform, (b) link deflections and joint variations in the ith leg.

in the passive revolute joint angles and those related to the actuator and link deflections, namely,

$$\$_O^i = \mathbf{J}_\theta^i \Delta \mathbf{u}_i + \mathbf{J}_q^i \Delta \mathbf{q}_i \qquad (15)$$

with

$$\mathbf{J}_\theta^i = \begin{bmatrix} \hat{\$}_A^i & \hat{\$}_{u1}^i & \hat{\$}_{u2}^i & \hat{\$}_{u3}^i & \hat{\$}_{u4}^i & \hat{\$}_{u5}^i & \hat{\$}_{u6}^i \end{bmatrix} \quad (16a)$$

$$\mathbf{J}_q^i = \begin{bmatrix} \hat{\$}_B^i & \hat{\$}_C^i \end{bmatrix} \qquad (16b)$$

$$\Delta \mathbf{u}_i = \begin{bmatrix} \Delta \theta_i & \Delta u_1^i & \Delta u_2^i & \Delta u_3^i & \Delta u_4^i & \Delta u_5^i & \Delta u_6^i \end{bmatrix}^T \quad (16c)$$

$$\Delta \mathbf{q}_i = \begin{bmatrix} \Delta \psi_i & \Delta \xi_i \end{bmatrix}^T \qquad (16d)$$

Let the external wrench applied to the end of the ith leg be denoted by $\mathbf{f}_i$, the constitutive law of the ith leg can be expressed as

$$\mathbf{f}_i = \begin{bmatrix} \mathbf{K}_{rr} & \mathbf{K}_{rt} \\ \mathbf{K}_{rt}^T & \mathbf{K}_{tt} \end{bmatrix}_i \begin{bmatrix} \Delta \boldsymbol{\phi} \\ \Delta \mathbf{p} \end{bmatrix} \quad \rightarrow \quad \mathbf{f}_i = \mathbf{K}_i \$_O^i \qquad (17)$$

On the other hand, the wrench applied to the articulated joints in the ith leg being denoted by a vector $\boldsymbol{\tau}_i$, the equilibrium condition for the system is written as,

$$\mathbf{J}_\theta^{iT} \mathbf{f}_i = \boldsymbol{\tau}_i, \ \mathbf{J}_q^{iT} \mathbf{f}_i = \mathbf{0}, \ \Delta \mathbf{u}_i = \mathbf{K}_\theta^{i^{-1}} \boldsymbol{\tau}_i \qquad (18)$$

Combining Eqns. (15), (17) and (18), the kinetostatic model of the ith leg can be reduced to a system of two matrix equations, namely,

$$\begin{bmatrix} \mathbf{S}_\theta^i & \mathbf{J}_q^i \\ \mathbf{J}_q^{iT} & \mathbf{0}_{2\times2} \end{bmatrix} \begin{bmatrix} \mathbf{f}_i \\ \Delta \mathbf{q}_i \end{bmatrix} = \begin{bmatrix} \$_O^i \\ \mathbf{0}_{2\times1} \end{bmatrix} \qquad (19)$$

where the sub-matrix $\mathbf{S}_\theta^i = \mathbf{J}_\theta^i \mathbf{K}_\theta^{i^{-1}} \mathbf{J}_\theta^{iT}$ describes the spring compliance relative to the center of rotation, and the sub-matrix $\mathbf{J}_q^i$ takes into account the passive joint influence on the mobile platform motions. $\mathbf{K}_\theta^{i^{-1}}$ is a 7×7 matrix, describing the compliance of the virtual springs and taking the form:

$$\mathbf{K}_\theta^{i^{-1}} = \begin{bmatrix} \mathbf{K}_{act}^{i^{-1}} & \mathbf{0}_{1\times6} \\ \mathbf{0}_{6\times1} & \mathbf{K}_L^{i^{-1}} \end{bmatrix} \qquad (20)$$

where $\mathbf{K}_{act}^i$ corresponds to the stiffness of the ith actuator. $\mathbf{K}_L^i$ of size 6×6 is the stiffness matrix of the curved link in the ith leg, which is calculated by means of the Euler-Bernoulli stiffness model of a cantilever. In Figure 3(b), Δu_1, Δu_2 and Δu_3 show the three moment directions while Δu_4, Δu_5 and Δu_6 show the three force directions, thus, using Castigliano's theorem (Hibbeler, 1997), the compliance matrix of the curved link takes the form:

$$\mathbf{K}_L^{i^{-1}} = \begin{bmatrix} C_{11} & C_{12} & 0 & 0 & 0 & C_{16} \\ C_{12} & C_{22} & 0 & 0 & 0 & C_{26} \\ 0 & 0 & C_{33} & C_{34} & C_{35} & 0 \\ 0 & 0 & C_{34} & C_{44} & C_{45} & 0 \\ 0 & 0 & C_{35} & C_{45} & C_{55} & 0 \\ C_{16} & C_{26} & 0 & 0 & 0 & C_{66} \end{bmatrix} \qquad (21)$$

where the corresponding elements are given in Appendix A.

The matrix $\mathbf{J}_\theta^i$ of size 6×7 is the Jacobian matrix related to the virtual springs and $\mathbf{J}_q^i$ of 6×2, the one related to revolute joints in the ith leg. The Cartesian stiffness matrix $\mathbf{K}_i$ of the ith leg is obtained from Eqn. (19),

$$\mathbf{f}_i = \mathbf{K}_i \$_O^i \qquad (22)$$

where $\mathbf{K}_i$ is a 6×6 sub-matrix, which is extracted from the inverse of the 8×8 matrix on the left-hand side of Eqn. (19). From $\mathbf{f} = \sum_{i=1}^3 \mathbf{f}_i$, $\$_O = \$_O^i$ and $\mathbf{f} = \mathbf{K}\$_O$, the Cartesian stiffness matrix $\mathbf{K}$ of the system is found by simple addition, namely,

$$\mathbf{K} = \sum_{i=1}^3 \mathbf{K}_i \qquad (23)$$

115

3.3 Mass matrix

The mass in motion of the mechanism influences the dynamic performance, such as inertia, acceleration, etc., hence, formulating the mass matrix is one important procedure in the dynamic analysis. Mass matrix is the function of manipulator dimensions and material properties, i.e., link lengths, cross-sectional area, mass density. Generally, the manipulator mass matrix (inertia matrix) can be obtained on the basis of its kinetic energy. The total kinetic energy T includes the energy T_p of the mobile platform, T_l of the curved links and T_s of the slide units:

- The kinetic energy of the mobile platform is

$$T_p = \frac{1}{2} m_p \mathbf{v}_p^T \mathbf{v}_p + \frac{1}{2} \boldsymbol{\omega}^T \mathbf{I}_p \boldsymbol{\omega} \qquad (24)$$

with

$$\mathbf{v}_p = R \cos \beta \mathbf{p} \times \boldsymbol{\omega}, \ \mathbf{I}_p = \operatorname{diag} \left[I_{xx} \ I_{yy} \ I_{zz} \right] \quad (25)$$

where m_p is the mass of the mobile-platform and I_{xx}, I_{yy}, I_{zz} are the mass moments of inertia of the mobile-platform about x-, y-, z-axes, respectively.

- The kinetic energy of the curved links is

$$T_l = \frac{1}{2} \sum_{i=1}^3 \left(m_l \mathbf{v}_l^{i^T} \mathbf{v}_l^i + I_l \dot{\psi}_i^2 \right) \qquad (26)$$

with

$$\mathbf{v}_l^i = \frac{1}{2} R \left(\dot{\theta}_i \mathbf{w}_i \times \mathbf{u}_i + \mathbf{v}_i \times \boldsymbol{\omega} \right) \qquad (27a)$$

$$I_l = \frac{1}{2} m_l R^2 \left(1 - \frac{\sin \alpha_2 \cos \alpha_2}{\alpha_2} \right) \qquad (27b)$$

$$\dot{\psi}_i = -\frac{(\mathbf{u}_i \times \mathbf{v}_i) \cdot \boldsymbol{\omega}}{(\mathbf{u}_i \times \mathbf{w}_i) \cdot \mathbf{v}_i} = \mathbf{j}_{\psi i} \cdot \boldsymbol{\omega} \qquad (27c)$$

where m_l is the link mass and I_l is its mass moment of inertia about $\mathbf{w}_i$.

- The kinetic energy of the slide units is

$$T_s = \frac{1}{2} \left(I_g n_g^2 + m_s R_s^2 \right) \dot{\boldsymbol{\theta}}^T \dot{\boldsymbol{\theta}} \qquad (28)$$

where m_s is the mass of the slide unit and R_s is the distance from its mass center to z-axis. I_g is the mass moment of inertia of the pinion and n_g is the gear ratio.

Consequently, the SPM kinetic energy can be written in the following form

$$T = T_p + T_l + T_s = \frac{1}{2} \dot{\boldsymbol{\theta}}^T \mathbf{M} \dot{\boldsymbol{\theta}} \qquad (29)$$
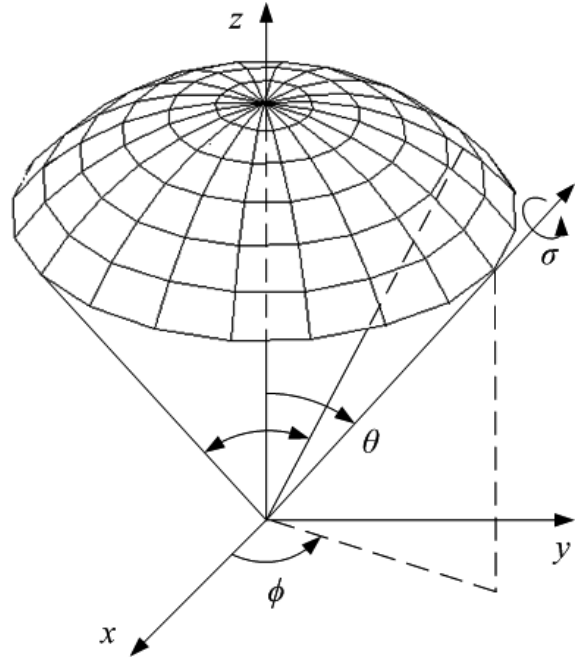
Figure 4: The representation of the regular workspace for the SPM with a pointing cone.

with the mass matrix $\mathbf{M}$ of the system is expressed as

$$\mathbf{M} = \left(m_s R_s^2 + I_g n_g^2 + \frac{1}{4} m_l R^2 \sin^2 \alpha_1 \right) \mathbf{1}_3$$
$$+ \mathbf{J}^T \left(\mathbf{I}_p + m_p R^2 \cos^2 \beta [\mathbf{p}]_\times^T [\mathbf{p}]_\times \right.$$
$$\left. + \frac{1}{4} m_l R^2 \sum_{i=1}^3 [\mathbf{v}_i]_\times^T [\mathbf{v}_i]_\times + I_l \sum_{i=1}^3 \mathbf{j}_{\psi i} \mathbf{j}_{\psi i}^T \right) \mathbf{J} \quad (30)$$

where $[\cdot]_\times$ stands for the skew-symmetric matrix whose elements are from the corresponding vector and $\mathbf{1}_3$ is the Identity matrix.

4 Design Optimization of the Spherical Parallel Manipulator

The inverse kinematic problem of the SPM can have up to eight solutions, i.e., the SPM can have up to eight working modes. Here, the diagonal terms b_i of the inverse Jacobian matrix $\mathbf{B}$ are supposed to be all negative for the SPM to stay in a given working mode. In the optimization procedure, criteria involving kinematic and kinetostatic/dynamic performances are considered to determine the mechanism configuration and the dimension and mass properties of the links. Moreover, the performances are evaluated over a regular shaped workspace free of singularity, which is specified as a minimum pointing cone of 90° opening with
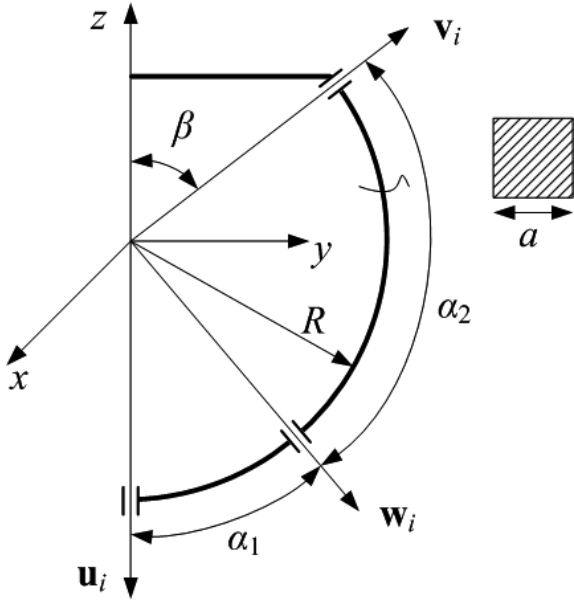
Figure 5: Design variables of the 3-R̲RR SPM.

360° full rotation, i.e., $\theta \geq 45°$ and $\sigma \in (-180°, 180°]$, see Figure 4.

4.1 Design variables

Variables α_1, α_2, β and γ are part of the geometric parameters of a 3-R̲RR SPM and $\gamma = 0$ for the manipulator under study. Moreover, the radius R of the link midcurve is another design variable and the cross section of the links is supposed to be a square of side length a. These variables are shown in Figure 5. As a consequence, the design variable vector is expressed as follows:

$$\mathbf{x} = [\alpha_1, \alpha_2, \beta, a, R] \qquad (31)$$

4.2 Objective functions

The kinematic performance is one of the major concerns in the manipulator design, of which a criterion is the evaluation of the dexterity of SPMs. A commonly used criterion to evaluate this kinematic performance is the global conditioning index (GCI) (Gosselin and Angeles, 1991), which describes the isotropy of the kinematic performance. The GCI is defined over a workspace Ω as

$$GCI = \frac{\int_\Omega \kappa^{-1}(\mathbf{J})\mathrm{d}W}{\int_\Omega \mathrm{d}W} \qquad (32)$$

where $\kappa(\mathbf{J})$ is the condition number of the kinematic Jacobian matrix (11). In practice, the GCI of a robotic

manipulator is calculated through a discrete approach as

$$GCI = \frac{1}{n}\sum_{i=1}^{n}\frac{1}{\kappa_i(\mathbf{J})} \qquad (33)$$

where n is the number of the discrete workspace points. As a result, the first objective function of the optimization problem is written as:

$$f_1(\mathbf{x}) = GCI \quad \rightarrow \quad \max \qquad (34)$$

Referring to the kinematic dexterity, an important criterion to evaluate the dynamic performance is dynamic dexterity, which is made on the basis of the concept of Generalized Inertia Ellipsoid (GIE) (Asada, 1983). In order to enhance the dynamic performance and to make acceleration isotropic, the mass matrix (30) should be optimized to obtain a better dynamic dexterity. Similar to GCI, a global dynamic index (GDI) is used to evaluate the dynamic dexterity, namely,

$$GDI = \frac{1}{n}\sum_{i=1}^{n}\frac{1}{\kappa_i(\mathbf{M})} \qquad (35)$$

where $\kappa_i(\mathbf{M})$ is the condition number of the mass matrix of the ith workspace point. Thus, the second objective function of the optimization problem is written as:

$$f_2(\mathbf{x}) = GDI \quad \rightarrow \quad \max \qquad (36)$$

4.3 Optimization constraints

In this section, the kinematic constraints, conditioning of the kinematic Jacobian matrix and accuracies due to the elastic deformation are considered. Constraining the conditioning of the Jacobian matrix aims to guarantee dexterous workspace free of singularity, whereas limits on accuracy consideration ensures that the mechanism is sufficiently stiff.

4.3.1 Kinematic constraints

According to the determination of design space reported in (Bai, 2010), the bounds of the parameter α_1, α_2 and β subject to the prescribed workspace are stated as:

$$45° \leq \beta \leq 90°, \ 45° \leq \alpha_1, \alpha_2 \leq 135° \qquad (37)$$

The sequence of the first, second and third slide units appearing on the circular guide counterclockwise is constant. In order to avoid collision, the angles θ_{ij} between the projections of vectors $\mathbf{w}_i$ and $\mathbf{w}_j$ in the xy quadrant, $i, j = 1, 2, 3, i \neq j$, as shown in Figure 6, have the minimum value, say 10°. To avoid collision
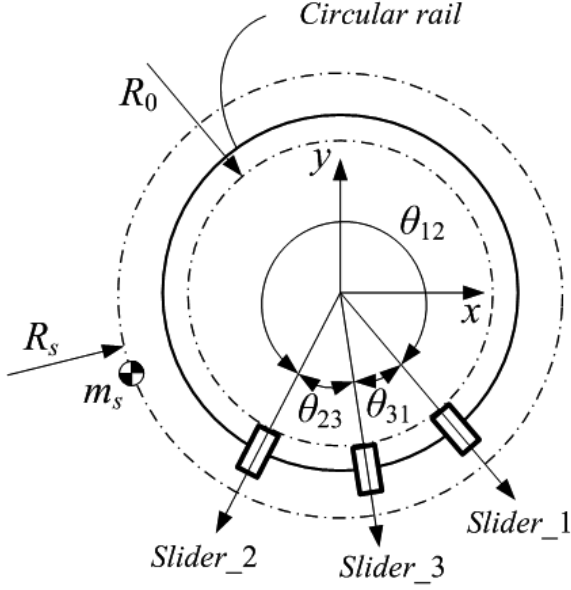
Figure 6: Slide unit configuration of the 3-DOF SPM.

and make the mechanism compact, the following constraints should be satisfied:

$$\theta_{12}, \theta_{23}, \theta_{31} \geq \epsilon_\theta = 10^{\mathrm{o}} \tag{38}$$
$$R_0 = 0.120\,\mathrm{m} \leq R\sin\alpha_1 \leq R_s = 0.200\,\mathrm{m}$$

Moreover, the SPM should not reach any singularity in its orientation workspace. Therefore, the following conditions should be satisfied.

$$det(\mathbf{A}) \geq \epsilon, \ b_i = (\mathbf{u}_i \times \mathbf{w}_i) \cdot \mathbf{v}_i \leq -\epsilon \tag{39}$$

where $\mathbf{A}$ is the forward Jacobian matrix of the manipulator defined in Eqn. (9) and $\epsilon > 0$ is a previously specified tolerance set to 0.001.

4.3.2 Conditioning number of the kinematic Jacobian matrix

Maximizing the GCI and constraining the kinematic Jacobian matrix cannot prevent the prescribed workspace away from ill-conditioned configurations. For the design optimization in order to achieve a dexterous workspace, the minimum of the inverse condition number of the kinematic Jacobian matrix $\kappa^{-1}(\mathbf{J})$, based on 2-norm, should be higher than a prescribed value throughout the workspace, say 0.1, namely,

$$min(\kappa^{-1}(\mathbf{J})) \geq 0.1 \tag{40}$$

4.3.3 Accuracy constraints

The accuracy constraints of the optimization problem for the SPM are related to the dimensions of

Table 1: The lower and upper bounds of the design variables $\mathbf{x}$.

	α_1 [deg]	α_2 [deg]	β [deg]	a [m]	R [m]
$\mathbf{x}_{lb}$	45	45	45	0.005	0.120
$\mathbf{x}_{ub}$	135	135	90	0.030	0.300

the curved link and the maximum positional deflection of the rotation center and angular deflection of the moving-platform subject to a given wrench applied on the latter. The control loop stiffness is $K_{act}^i = 10^6\,\mathrm{Nm/rad}$. Let the static wrench capability be specified as the eight possible combinations of moments $\mathbf{m} = [\pm10, \pm10, \pm10]\,\mathrm{Nm}$, while the allowable maximum positional and rotational errors for the workspace points are $1\,\mathrm{mm}$ and $2^{\mathrm{o}} = 0.0349\,\mathrm{rad}$, respectively, thus, the accuracy constraints can be written as:

$$\|\Delta\mathbf{p}\|_n = \sqrt{\Delta x_n^2 + \Delta y_n^2 + \Delta z_n^2} \leq \epsilon_p \tag{41}$$
$$\|\Delta\boldsymbol{\phi}\|_n = \sqrt{\Delta\phi_{x,n}^2 + \Delta\phi_{y,n}^2 + \Delta\phi_{z,n}^2} \leq \epsilon_r$$

where the linear and angular displacements are computed from $\$_O = \mathbf{K}^{-1}\mathbf{f}$ with the Cartesian stiffness matrix (23) and $\epsilon_p = 1\,\mathrm{mm}$, $\epsilon_r = 0.0349\,\mathrm{rad}$.

4.4 Formulation of the multiobjective optimization problem

Mathematically, the multi-objective design optimization problem for the spherical parallel manipulator can be formulated as:

$$\begin{aligned}
\text{maximize} \quad & f_1(\mathbf{x}) = GCI \tag{42}\\
\text{maximize} \quad & f_2(\mathbf{x}) = GDI\\
\text{over} \quad & \mathbf{x} = [\alpha_1, \alpha_2, \beta, a, R]\\
\text{subject to} \quad & g_1 : \theta \geq 45^{\mathrm{o}}\\
& g_2 : R_0 \leq R\sin\alpha_1 \leq R_s\\
& g_3 : \theta_{12}, \theta_{23}, \theta_{31} \geq \epsilon_\theta = 10^{\mathrm{o}}\\
& g_4 : det(\mathbf{A}) \geq \epsilon, \ (\mathbf{u}_i \times \mathbf{w}_i) \cdot \mathbf{v}_i \leq -\epsilon\\
& g_5 : min(\kappa^{-1}(\mathbf{J})) \geq 0.1\\
& g_6 : \sqrt{\Delta x_n^2 + \Delta y_n^2 + \Delta z_n^2} \leq \epsilon_p\\
& g_7 : \sqrt{\Delta\phi_{x,n}^2 + \Delta\phi_{y,n}^2 + \Delta\phi_{z,n}^2} \leq \epsilon_r\\
& \mathbf{x}_{lb} \leq \mathbf{x} \leq \mathbf{x}_{ub}\\
& i = 1, 2, 3
\end{aligned}$$

where $\mathbf{x}_{lb}$ and $\mathbf{x}_{ub}$, respectively, are the lower and upper bounds of the variables $\mathbf{x}$ given by Table 1.

Table 2: Algorithm parameters of the implemented NSGA-II

Population size	Generation	Directional crossover probability	Crossover probability	Mutation probability	Distribution index
40	200	0.5	0.9	0.1	20

Table 3: Three Pareto-optimal solutions

Design ID	Variables					Objectives	
	α_1 [deg]	α_2 [deg]	β [deg]	a [m]	R [m]	GCI	GDI
I	56.2	81.0	89.8	0.0128	0.1445	0.366	0.711
II	51.6	84.3	89.9	0.0133	0.1533	0.453	0.665
III	47.2	90.8	89.2	0.0127	0.1641	0.536	0.625

4.5 Pareto-optimal solutions

For the proposed SPM, the actuation transmission mechanism is a combination of actuator of model RE 35 GB and gearhead of model GP 42 C from Maxon (Maxon, 2012) and a set of gear ring-pinion with ratio $n_g = 8$. Moreover, the components are supposed to be made of steel, thus, $E = 210$ Gpa, $\nu = 0.3$. Moreover, the moving platform is supposed to be a regular triangle, thus, the MP and link masses are given by

$$m_p = \frac{3\sqrt{3}}{4}\rho h R^2 \sin^2 \beta, \; m_l = \rho a^2 R \alpha_2 \qquad (43)$$

where ρ is the mass density and $h = 0.006$ m is the thickness of the moving platform. The total mass m_s of each slide unit, including the mass of the actuator, gearhead, pinion and the manufactured components, is equal to $m_s = 2.1$ kg.

The previous formulated optimization problem (42) is solved by the genetic algorithm NSGA-II (Deb et al., 2002) with *Matlab*, of which the algorithm parameters are given in Table 2.

The Pareto front of the formulated optimization problem for the SPM is shown in Figure 7 and three optimal solutions, i.e., two extreme and one intermediate, are listed in Table 3.

Figure 8 illustrates the variational trends as well as the inter-dependency between the objective functions and design variables by means of a scatter matrix. The lower triangular part of the matrix represents the correlation coefficients whereas the upper one shows the corresponding scatter plots. The diagonal elements represent the probability density charts of each variable. The correlation coefficients vary from -1 to 1. Two variables are strongly dependent when their correlation coefficient is close to -1 or 1 and independent when the latter is null. Figure 8 shows:

- both objectives functions GCI and GDI are
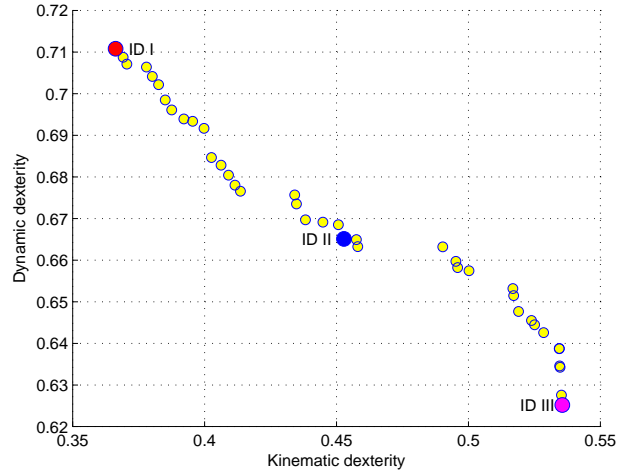
Figure 7: The Pareto front of the multiobjective optimization problem for the SPM.

strongly dependent as their correlation coefficient is equal to -0.975;

- both objectives functions GCI and GDI are strongly dependent on all design variables as all of the corresponding correlation coefficients are greater than 0.6;

- GCI is slightly more dependent than GDI of the design variables as all the corresponding correlation coefficients of former are greater than those of latter;

- GDI is less dependent on the design variables β and a than the other variables although the two former variables influence the SPM mass, this is due to the large portion of the slide unit mass in the total mechanism mass.
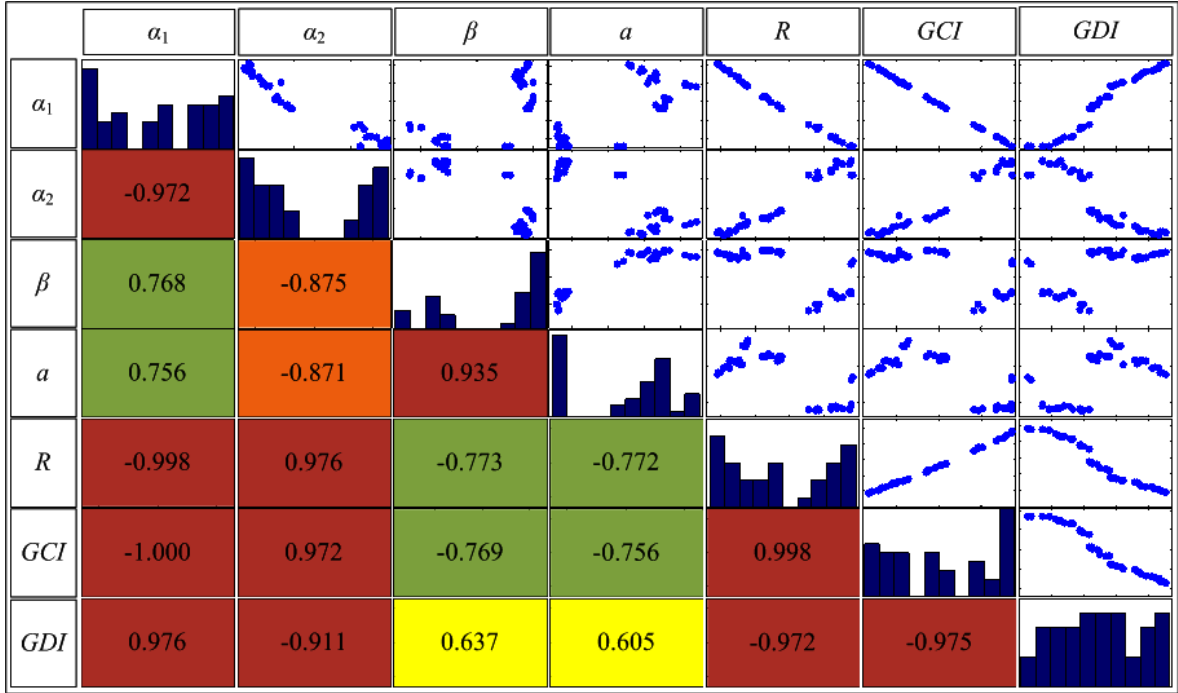
Figure 8: Scatter matrix for the objective functions and the design variables.
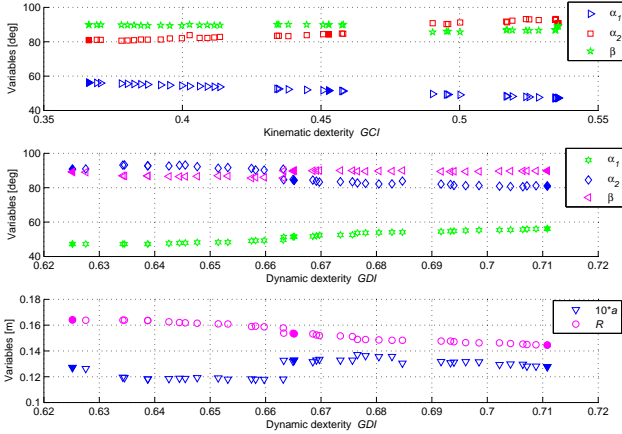
Figure 9: Design variables as functions of objectives for the Pareto-optimal solutions.

Figure 9 displays the design variables as functions of the objectives. It is noteworthy that the higher GCI, the lower α_1, conversely, the higher GDI, the higher α_1. This phenomenon is opposite with respect to variable α_2. The design variable β converges to 90º approximately, which indicates that $\beta = 90$º is the preferred geometric parameter for the SPM under study. The lower link midcurve R and higher a lead to higher GDI. The three sets of of design variables corresponding to the three Pareto-optimal solutions depicted in Table 3 are shown in Figure 9 with solid markers.

5 Conclusions

In this paper, the geometric synthesis of spherical parallel manipulators is discussed. A multiobjective design optimization problem based on the genetic algorithm was formulated in order to determine the mechanism optimum structural and geometric parameters. The objective functions were defined on the basis of the criteria of both kinematic and kinetostatic/dynamic performances. This approach is illustrated with the optimum design of an unlimited-roll spherical parallel manipulator, aiming at maximizing the kinematic and dynamic dexterities to achieve relatively better kinematic and dynamic performances simultaneously. It is found that the parameter β being equal to 90º is a preferred structure for the SPM under study. Finally, the Pareto-front was obtained to show the approximation of the optimal solutions between the various (antagonistic) criteria, subject to the dependency of the performance. The future work will aim to maximize the orientation workspace and optimize the cross-section type of the curved links.

References

Altuzarra, O., Salgado, O., Hernandez, A., and Angeles, J. Multiobjective optimum design of a symmetric parallel schönflies-motion generator.

ASME J. Mechanical Design, 2009. 131(3):031002. doi:10.1115/1.3066659.

Asada, H. A geometrical representation of manipulator dynamics and its application to arm design. *ASME J. Dynamic Systems, Measurement and Control*, 1983. 105(3):131–142. doi:10.1115/1.3140644.

Asada, H. and Granito, J. Kinematic and static characterization of wrist joints and their optimal design. In *IEEE International Conference on Robotics and Automation*. pages 244–250, 1985. doi:10.1109/ROBOT.1985.1087324.

Bai, S. Optimum design of spherical parallel manipulator for a prescribed workspace. *Mechanism and Machine Theory*, 2010. 45(2):200–211. doi:10.1016/j.mechmachtheory.2009.06.007.

Bai, S., Hansen, M. R., and Andersen, T. O. Modelling of a special class of spherical parallel manipulators with Euler parameters. *Robotica*, 2009. 27(2):161–170. doi:10.1017/S0263574708004402.

Bonev, I. A. Direct kinematics of zero-torsion parallel mechanisms. In *IEEE International Conference on Robotics and Automation*. Pasadena, California, USA, pages 3851–3856, 2008. doi:10.1109/ROBOT.2008.4543802.

Bonev, I. A. and Gosselin, C. M. Analytical determination of the workspace of symmetrical spherical parallel mechanisms. *IEEE Transactions on Robotics*, 2006. 22(5):1011–1017. doi:10.1109/TRO.2006.878983.

Caro, S., Chablat, D., Ur-Rehman, R., and Wenger, P. Multiobjective design optimization of 3-PRR planar parallel manipulators. In *Global Product Development*, pages 373–383. Springer-Verlag Berlin Heidelberg, 2011. doi:10.1007/978-3-642-15973-2_37.

Cavallo, E. and Michelini, R. C. A robotic equipment for the guidance of a vectored thrustor. In *35th International Symposium on Robotics*. Paris, France, 2004.

Ceccarelli, M., Carbone, G., and Ottaviano, E. Multi criteria optimum design of manipulators. *In Bulletin of the Polish Academy of Technical Sciences*, 2005. 53(1):9–18.

Chaker, A., Mlika, A., Laribi, M. A., Romdhane, L., and Zeghloul, S. Synthesis of spherical parallel manipulator for dexterous medical task. *Frontiers of Mechanical Engineering*, 2012. 7(2):150–162. doi:10.1007/s11465-012-0325-4.

Deb, K., Pratap, A., Agarwal, S., and Meyarivan, T. A fast and elitist multiobjective genetic algorithm: NSGA-II. *IEEE Trans. Evolutionary Computation*, 2002. 6(2):182–197. doi:10.1109/4235.996017.

Durand, S. L. and Reboulet, C. Optimal design of a redundant spherical parallel manipulator. *Robotica*, 1997. 15(4):399–405. doi:10.1017/S0263574797000490.

Gosselin, C. M. and Angeles, J. The optimum kinematic design of a spherical three-degree-of-freedom parallel manipulator. *ASME J. Mechanisms, Transmissions, and Automation in Design*, 1989. 111:202–207. doi:10.1115/1.3258984.

Gosselin, C. M. and Angeles, J. A global performance index for the kinematic optimization of robotic manipulators. *ASME J. Mechanical Design*, 1991. 113(3):220–226. doi:10.1115/1.2912772.

Gosselin, C. M. and Hamel, J. F. The Agile Eye: a high-performance three-degree-of-freedom camera-orienting device. In *IEEE International Conference on Robotics and Automation*. San Diego, CA, pages 781–786, 1994. doi:10.1109/ROBOT.1994.351393.

Hao, F. and Merlet, J.-P. Multi-criteria optimal design of parallel manipulators based on interval analysis. *Mechanism and Machine Theory*, 2005. 40(2):157–171. doi:10.1016/j.mechmachtheory.2004.07.002.

Hay, A. M. and Snyman, J. A. Methodologies for the optimal design of parallel manipulators. *Inter. J. Numerical Methods in Engineering*, 2004. 59(11):131–152. doi:10.1002/nme.871.

Hibbeler, R. C. *Mechanics of Materials*. Prentice Hall, 1997.

Huang, T., Gosselin, C. M., Whitehouse, D. J., and Chetwynd, D. G. Analytic approach for optimal design of a type of spherical parallel manipulators using dexterous performance indices. *IMechE. J. Mechan. Eng. Sci.*, 2003. 217(4):447–455. doi:10.1243/095440603321509720.

Kong, K. and Gosselin, C. M. Type synthesis of three-degree-of-freedom spherical parallel manipulators. *Inter. J. Robotics Research*, 2004. 23(3):237–245. doi:10.1177/0278364904041562.

Krefft, M. and Hesselbach, J. Elastodynamic optimization of parallel kinematics. In *Proceedings of the IEEE International Conference on Automation Science and Engineering*. Edmonton, AB, Canada, pages 357–362, 2005. doi:10.1109/COASE.2005.1506795.

Li, T. and Payandeh, S. Design of spherical parallel mechanisms for application to laparoscopic surgery. *Robotica*, 2002. 20(2):133–138. doi:10.1017/S0263574701003873.

Liu, X. J., Jin, Z. L., and Gao, F. Optimum design of 3-dof spherical parallel manipulators with respect to the conditioning and stiffness indices. *Mechanism and Machine Theory*, 2000. 35(9):1257–1267. doi:10.1016/S0094-114X(99)00072-5.

Lou, Y., Liu, G., Chen, N., and Li, Z. Optimal design of parallel manipulators for maximum effective regular workspace. In *Proceedings of the IEEE/RSJ International Conference on Intelligent Robots and Systems*. Alberta, pages 795–800, 2005. doi:10.1109/IROS.2005.1545144.

Maxon. *Maxon Motor and Gearhead products catalog.* 2012. URL http://www.maxonmotor.com/maxon/view/catalog/.

Merlet, J.-P. Jacobian, manipulability, condition number, and accuracy of parallel robots. *ASME J. Mechanical Design*, 2006a. 128(1):199–206. doi:10.1115/1.2121740.

Merlet, J.-P. *Parallel Robots.* Kluwer, Norwell, 2006b.

Pashkevich, A., Chablat, D., and Wenger, P. Stiffness analysis of overconstrained parallel manipulators. *Mechanism and Machine Theory*, 2009. 44(5):966–982. doi:10.1016/j.mechmachtheory.2008.05.017.

Stamper, R. E., Tsai, L.-W., and Walsh, G. C. Optimization of a three-dof translational platform for well-conditioned workspace. In *Proceedings of the IEEE International Conference on Robotics and Automation.* Albuquerque, NM, pages 3250–3255, 1997. doi:10.1109/ROBOT.1997.606784.

Stock, M. and Miller, K. Optimal kinematic design of spatial parallel manipulators: Application of linear delta robot. *ASME J. Mechanical Design*, 2003. 125(2):292–301. doi:10.1115/1.1563632.

Tsai, L.-W. The Jacobian analysis of parallel manipulators using reciprocal screws. In J. Lenarčič and M. L. Husty, editors, *Advances in Robot Kinematics: Analysis and Control*, pages 327–336. Kluwer Academic Publishers, 1998.

Appendix A

The elements of the compliance matrix (21) for the curved beam

$$C_{11} = \frac{R}{2}\left(\frac{s_1}{GI_x} + \frac{s_2}{EI_y}\right) \tag{A-1a}$$

$$C_{12} = \frac{s_8 R}{2}\left(\frac{1}{GI_x} - \frac{1}{EI_y}\right) \tag{A-1b}$$

$$C_{16} = \frac{R^2}{2}\left(\frac{s_2}{EI_y} - \frac{s_7}{GI_x}\right) \tag{A-1c}$$

$$C_{22} = \frac{R}{2}\left(\frac{s_2}{GI_x} + \frac{s_1}{EI_y}\right) \tag{A-1d}$$

$$C_{26} = \frac{R^2}{2}\left(\frac{s_4}{GI_x} - \frac{s_2}{EI_y}\right) \tag{A-1e}$$

$$C_{33} = \frac{R\alpha_2}{EI_z} \tag{A-1f}$$

$$C_{34} = \frac{s_5 R^2}{EI_z} \tag{A-1g}$$

$$C_{35} = \frac{s_6 R^2}{EI_z} \tag{A-1h}$$

$$C_{44} = \frac{R}{2A}\left(\frac{s_1}{E} + \frac{s_2}{G}\right) + \frac{s_3 R^3}{2EI_z} \tag{A-1i}$$

$$C_{45} = \frac{s_8 R}{2A}\left(\frac{1}{E} - \frac{1}{G}\right) + \frac{s_4 R^3}{2EI_z} \tag{A-1j}$$

$$C_{55} = \frac{R}{2A}\left(\frac{s_1}{G} + \frac{s_2}{E}\right) + \frac{s_2 R^3}{2EI_z} \tag{A-1k}$$

$$C_{66} = \frac{R\alpha_2}{GA} + \frac{R^3}{2}\left(\frac{s_3}{GI_x} + \frac{s_2}{EI_y}\right) \tag{A-1l}$$

with

$$s_1 = \alpha_2 + \sin\alpha_2\cos\alpha_2 \tag{A-2a}$$
$$s_2 = \alpha_2 - \sin\alpha_2\cos\alpha_2 \tag{A-2b}$$
$$s_3 = 3\alpha_2 + \sin\alpha_2\cos\alpha_2/2 - 4\sin\alpha_2 \tag{A-2c}$$
$$s_4 = 1 - \cos\alpha_2 - \sin^2\alpha_2/2 \tag{A-2d}$$
$$s_5 = \sin\alpha_2 - \alpha_2 \tag{A-2e}$$
$$s_6 = \cos\alpha_2 - 1 \tag{A-2f}$$
$$s_7 = 2\sin\alpha_2 - \alpha_2 - \sin\alpha_2\cos\alpha_2 \tag{A-2g}$$
$$s_8 = -\sin^2\alpha_2 \tag{A-2h}$$

where E is the Young's modulus and $G = E/2(1+\nu)$ is the shear modulus with the Poisson's ratio ν. I_x, I_y and I_z are the moments of inertia, respectively. A is the area of the cross-section.